Journal of the Physical Society of Japan
Vol. 67, No. 2, February, 1998, pp. 612-621

Low Temperature Properties of the Magnetic Semiconductor TmTe

Takeshi MATSUMURA*, Shintaro NAKAMURA[1], Terutaka GOTO[2], Hiroshi AMITSUKA[3], Kazuyuki MATSUHIRA[3], Toshiro SAKAKIBARA[3] and Takashi SUZUKI

Department of Physics, Graduate School of Science, Tohoku University, Sendai 980-77
[1]*Center for Low Temperature Science, Tohoku University, Katahira, Sendai 980-77*
[2]*Graduate School of Science and Technology, Niigata University, Niigata 950-21*
[3]*Division of Physics, Graduate School of Science, Hokkaido University, Sapporo 060*

(Received August 14, 1997)

The magnetic susceptibility, elastic constant, specific heat and magnetization of the magnetic semiconductor TmTe have been measured in detail. A phase transition which is likely to be an antiferro quadrupolar ordering was found to occur at 1.8 K. The specific heat measurements under magnetic fields along the three main crystal axes revealed the unusual characters of this phase transition. The $(H-T)$ phase diagram below 5 T is very similar to that of the antiferro quadrupolar ordering in CeB_6. Above 5 T, however, the phase line for $H \parallel [100]$ begins to close toward $T = 0$ K. The physical properties in the paramagnetic region at high temperatures are discussed in the mean field approximation. The theoretical fitting of the elastic softening indicates the antiferro inter-ionic quadrupolar interactions. However, the mean field theory can not explain the specific heat results.

KEYWORDS: TmTe, antiferro quadrupolar ordering, magnetic phase diagram

§1. Introduction

The thulium monochalcogenides TmX (X=S, Se and Te) with the NaCl structure have attracted much interest since the discovery of their anomalous physical properties associated with the degree of valence of the Tm ions. TmTe is a magnetic semiconductor with predominantly divalent Tm ions. This is apparent from its lattice parameter, magnetic susceptibility and electrical resistivity.[1)] The $4f^{13}$ level is located within the energy gap between the filled Te-$5p$ valence band and the empty Tm-$5d$ conduction band.[2-4)] The gap between the $4f$ level and the bottom of the conduction band has been estimated to be 0.35 eV.[5)]

In TmSe, the $4f$ level overlaps with the conduction band due to the smaller lattice parameter and a homogeneous intermediate valence state appears. Both the lattice parameter and the Curie constant have intermediate values between Tm^{2+} and Tm^{3+} configurations.[1)] The electrical resistivity shows a Kondo-like $\log T$ dependence at high temperatures followed by a sharp increase at the antiferro magnetic ordering temperature $T_N = 3.5$ K.[6,7)] This resistivity jump is thought to be a transition into an insulating state.[8)] The application of a weak magnetic field about 5 kG leads to a phase transition into a ferromagnetic metal.[9-11)] TmSe is also known as a unique intermediate valence rare earth compound that orders magnetically. Unlike Ce, Sm, Eu and Yb, both 2+ and 3+ configurations of Tm have magnetic ground state with $J = 7/2$ and $J = 6$, respectively. This fact is thought to be the origin of the occurrence of the magnetic ordering and other distinctive features in TmSe. One of the remarkable features is that the quasielastic linewidth in neutron scattering is almost temperature independent at high temperatures but it follows $\sim k_B T$ below 80 K. Furthermore, an inelastic peak becomes recognizable at 6 meV below 60 K, which shifts to a clearly separated peak at 10 meV at the lowest temperature.[12-14)] The origin of these anomalous behavior has not yet been understood. The electrical resistivity of TmS also shows a $\log T$ dependence although TmS is a metal with almost trivalent valence of Tm.[15,16)] Temperature dependence of the quasielastic linewidth and the inelastic peak also show similar behavior as those for TmSe.[17)]

The application of an external pressure on TmTe also leads to a similar situation in which the $4f$ level overlaps with the conduction band.[18)] Resistivity of TmTe also shows $\log T$ dependence after the semiconductor to metal transition at 2 GPa.[19)]

TmTe has been considered to be a simple divalent magnetic semiconductor so far. To understand the anomalous valence fluctuation state in TmSe, TmS and TmTe at high pressure, it is important to understand TmTe at an ambient pressure, which is the purpose of the present paper.

The Hund's rule ground multiplet of $4f^{13}$ configuration in TmTe is $J = 7/2$, which splits into Γ_8 quartet, Γ_7 doublet and Γ_6 doublet under the cubic crystalline electric field (CEF). A Schottky specific heat peak appears around 5 K, indicating the total CEF splitting is about 15 K.[1)] Ott *et al.* have proposed a level scheme of $\Gamma_8(0) - \Gamma_7(10) - \Gamma_6(16\ \mathrm{K})$ from the elastic constant and thermal expansion results.[20,21)] Recent inelastic neutron scattering experiment also supports the Γ_8 ground state and the small total splitting less than 20 K.[22)] The type II antiferro magnetic (AFM) ordering occurs at a low temperature. The transition temperature was reported

* E-mail: matsu@mail.cc.tohoku.ac.jp

to be 0.43 K from neutron scattering and 0.235 K from magnetic susceptibility.[1,23,24]

Recently, it was found that TmTe undergoes another phase transition at 1.8 K.[25,26] This transition has been ascribed to an ordering among the quadrupolar moments of the localized $4f$ electrons. This paper reports the low temperature physical properties of TmTe at an ambient pressure in detail, especially in the temperature range including this newly discovered phase transition, and discusses the role of the quadrupolar moments and their ordering.

§2. Samples and Experiments

We have prepared the samples by synthesizing high purity thulium metal (Ames Laboratory, USA) and 6N tellurium (High Purity Chemicals Co Ltd., Japan) directly in vacuum sealed tungsten crucibles with a high frequency induction furnace. No pre-reaction in quartz tubes was performed to avoid contamination by the quartz tube. It is possible to seal tungsten crucibles by electron beam welding without any loss of tellurium because of its relatively high melting point compared with selenium or sulfur. For selenides and sulfides, pre-reaction in quartz tube is needed to avoid evaporation while welding the crucible. Single crystal was grown by moving down the crucible out of the high frequency coil at a speed of about 2 mm/hour from a temperature about 1900°C. The size of the obtained sample was $\sim$1 cm^3 and the color was dark blue. The lattice parameter was 6.354±0.004 Å. The effective Bohr magneton and the paramagnetic Curie temperature deduced from the fitting of the inverse magnetic susceptibility between 100 K and 300 K were 4.56 μ_B and 1.8 K, respectively. The electrical resistivity varied from a few $\Omega\cdot$cm at room temperature to $10^6 \sim 10^7$ $\Omega\cdot$cm at 20 K. These basic properties indicate the high quality of the sample. This sample is named TmTe(9602).

All the experimental results described in this paper are those for TmTe(9602) except the elastic constant results. The elastic constants were measured with another sample named TmTe(9309), which was synthesized from commercial thulium metal. The basic properties of TmTe(9309) are described in previous papers.[25-27]

The magnetic susceptibility was measured with a SQUID magnetometer from 1.8 K to 300 K and with an AC technique below 5 K. The amplitude and the frequency of the alternating magnetic field were 4 Gauss and 80 Hz, respectively. The absolute values of the AC susceptibility data were determined from the fit to the SQUID result from 1.8 K to 5 K. The sound velocity was measured with an ultrasonic apparatus based on the phase comparison method. The absolute sound velocity was determined from the delay time of the ultrasonic echoes with an accuracy of several percent. The elastic constant C_{ij} was calculated from the relation $C_{ij} = \rho v^2$ where ρ is the density of the crystal and v is the sound velocity. The magnetization was measured with an extraction method. The sample was shaped into a sphere to correct the demagnetization field. The specific heat was measured with a quasi-adiabatic heat pulse method.

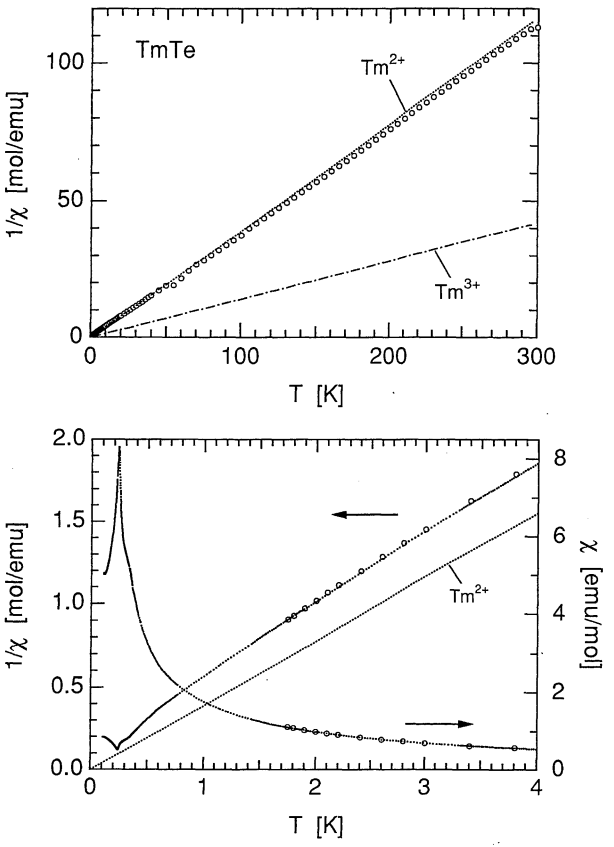

Fig. 1. Temperature dependence of the magnetic susceptibility of TmTe. Circles and dots represent the results measured with a SQUID magnetometer and with an AC technique, respectively. The dotted and the single dotted lines represent the theoretical inverse susceptibility for free Tm^{2+} and Tm^{3+} ions, respectively.

§3. Experimental Results

3.1 Magnetic susceptibility and elastic constants

Figure 1 shows the temperature dependence of the magnetic susceptibility. The $1/\chi(T)$ at high temperatures well follows the theoretical line for a free Tm^{2+} ion, indicating that the $4f$ electrons are well localized and that the valence of the Tm ions is almost divalent. The existence of the trivalent component, however, can not be denied. The $1/\chi(T)$ crosses and goes over the theoretical line below 30 K. This deviation from the Curie-Weiss behavior might be related with the anomaly that reflect the CEF levels. However, the splitting is expected to be very small even if it existed. The $\chi(T)$ exhibited a sharp cusp at $T_N = 0.236$ K. This Néel temperature is in accord with the previous result of 0.235 K from AC susceptibility but is lower than 0.43 K from neutron scattering.[1,23,24] This point will be discussed in the final section of this paper. It should also be noted that a small shoulder, which is not an experimental error, was observed around 0.4 K.

Figures 2 and 3 show the temperature dependence of the elastic constants. All of the three modes, C_{11}, $(C_{11}-C_{12})/2$ and C_{44}, showed softening with decreasing temperature. In particular, C_{44} showed a large softening of 20%. The bulk modulus C_B was calculated from the results of C_{11} and $(C_{11}-C_{12})/2$ using the relation

Table I. Irreducible representations of the strains, operator equivalents of the multipole moments up to second order ($l = 2$), and the corresponding elastic constants for a cubic crystal.

	$\varepsilon_{\Gamma\gamma}$	$O_{\Gamma\gamma}$	C_Γ
Γ_1	$\varepsilon^\alpha = (\varepsilon_{xx}+\varepsilon_{yy}+\varepsilon_{zz})/\sqrt{3}$	$O_B = J_x^2+J_y^2+J_z^2$	$C_{11}+2C_{12}=3C_B$
Γ_3	$\varepsilon_1^\gamma = (2\varepsilon_{zz}-\varepsilon_{xx}-\varepsilon_{yy})/\sqrt{6}=\varepsilon_u$ $\varepsilon_2^\gamma = (\varepsilon_{xx}-\varepsilon_{yy})/\sqrt{2}=\varepsilon_v$	$O_2^0 = \{3J_z^2-J(J+1)\}/\sqrt{3}$ $O_2^2 = J_x^2-J_y^2$	$(C_{11}-C_{12})$
Γ_5	$\varepsilon_1^\varepsilon = \sqrt{2}\varepsilon_{yz}$ $\varepsilon_2^\varepsilon = \sqrt{2}\varepsilon_{zx}$ $\varepsilon_3^\varepsilon = \sqrt{2}\varepsilon_{xy}$	$O_{yz} = J_yJ_z+J_zJ_y$ $O_{zx} = J_zJ_x+J_xJ_z$ $O_{xy} = J_xJ_y+J_yJ_x$	$2C_{44}$

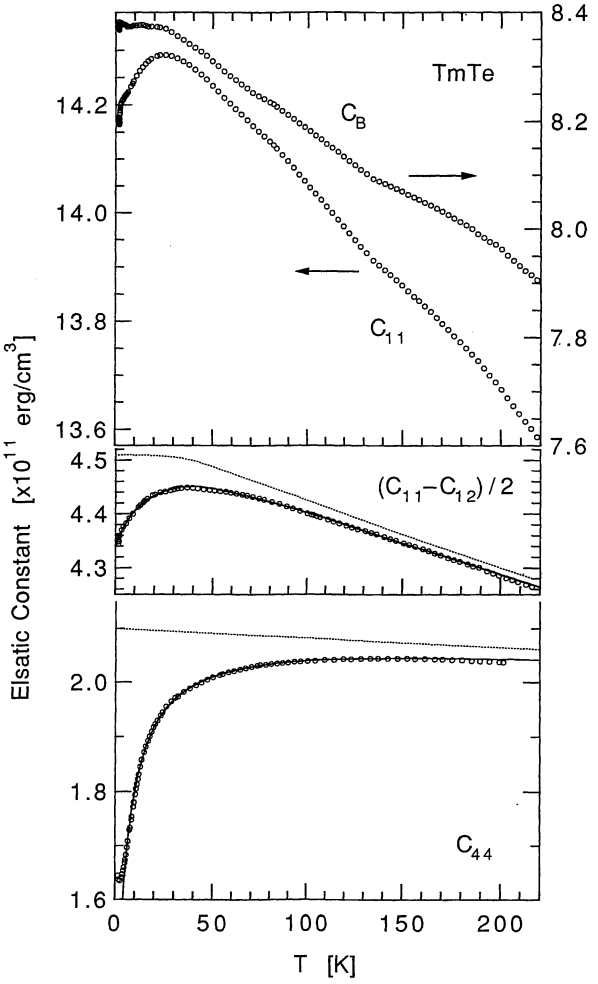

Fig. 2. Temperature dependence of the elastic constants of TmTe. The lines for $(C_{11}-C_{12})/2$ and C_{44} are the theoretical fits with eq. (3.2). The dotted lines are the estimated background elastic constants.

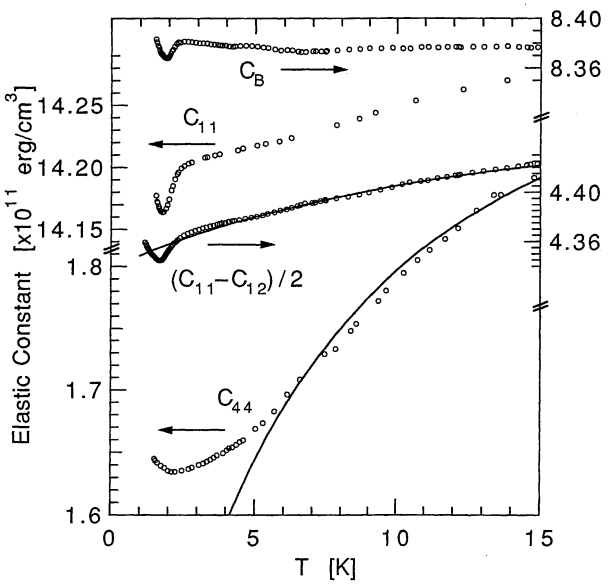

Fig. 3. Low temperature part of the elastic constants of TmTe.

$C_B = (C_{11}+2C_{12})/3$. In contrast to the other three elastic constants, C_B exhibited a quite normal temperature dependence.

The elastic softening of a localized f electron system can usually be understood as the quadrupolar response of the system to an external strain.[28-31] This effect has its origin in the modulation of the CEF by the strain. The lowest order term of this perturbation can be written as

$$\sum_{\Gamma\gamma} g_\Gamma O_{\Gamma\gamma}\varepsilon_{\Gamma\gamma}. \tag{3.1}$$

$\Gamma\gamma$ represents the irreducible representation and those for cubic symmetry are summarized in Table I. $O_{\Gamma\gamma}$ is the operator equivalent of a quadrupolar moment except O_B which represents a monopole. g_Γ is the coupling constant and does not depend on γ.

The second derivative of the free energy with respect to $\varepsilon_{\Gamma\gamma}$ gives the corresponding elastic constant C_Γ. Taking into account the inter-ionic quadrupolar interaction in the mean field approximation, we obtain the temperature dependence of the elastic constant as

$$C_\Gamma(T) = C_\Gamma^0(T) - \frac{Ng_\Gamma^2\chi_\Gamma^{st}(T)}{1-g_\Gamma'\chi_\Gamma^{st}(T)}, \tag{3.2}$$

where g_Γ' is the inter-ionic quadrupolar coupling constant and N is the number of ions in a unit volume. χ_Γ^{st} is the single ion quadrupolar strain susceptibility, which can be written, for a cubic system, as

$$\chi_\Gamma^{st}(T) = \sum_{ik}\frac{e^{-E_{ik}^{(0)}/k_BT}}{Z}\left(\frac{1}{k_BT}|\langle ik|O_\Gamma|ik\rangle|^2 - 2\sum_{jl}\frac{|\langle ik|O_\Gamma|jl\rangle|^2}{E_i-E_j}\right), \tag{3.3}$$

where $|ik\rangle$ represents the k-th eigenfunction of the i-th CEF level. C_Γ^0 in eq. (3.2) is the background elastic con-

stant without the contribution of the f electrons. Variation in C_Γ^0 originates mainly from anharmonic effects of the crystal. The second term of eq. (3.2) gives the effect of the localized f electrons under CEF. When the ground state is degenerate with respect to the quadrupolar moment O_Γ, a softening in the corresponding elastic constant is expected to occur due to the non-zero Curie term. The strain susceptibility of a monopole, an isotropic charge distribution, is zero and gives no anomaly to C_B.

The above formalism is very similar to that of the magnetic susceptibility. If we replace O_Γ in eq. (3.3) with J_z and multiply $g^2\mu_B^2$, we obtain the temperature dependence of the magnetic susceptibility of a localized f electron system with cubic symmetry. If the ground state is magnetically degenerated, the magnetic susceptibility shows a Curie type temperature dependence. These two kinds of susceptibility, when they have non zero Curie term, diverge with decreasing temperature until the degeneracy of the ground state is lifted. In TmTe, the softening in the elastic constants stops at 1.8 K and shows the cusp, while the magnetic susceptibility shows no anomaly at this temperature and continues to increase until T_N. *This fact strongly indicates that only the degeneracy of the quadrupolar moment is lifted while the degeneracy of the magnetic moment, Kramers doublet, remains below the phase transition at 1.8 K.* The magnetic degeneracy is not lifted until the magnetic ordering temperature where the magnetic susceptibility stops increasing and shows the cusp.

We have analyzed the elastic softening with eq. (3.2) assuming all the Tm ions are divalent. The fitting results are shown by the solid lines in the Figs. 2 and 3. The background elastic constants were determined so that the high temperature part of the softening, $C_\Gamma^0(T) - C_\Gamma(T)$, followed the Curie-Weiss behavior. The CEF splitting was assumed to be zero in this fitting because the total splitting is very small. The obtained parameter was as follows: $|g_{\Gamma_3}| = 63$ K, $g_{\Gamma_3}' = -0.25$ K, $|g_{\Gamma_5}| = 81$ K and $g_{\Gamma_5}' = -0.076$ K.

Inelastic neutron scattering was recently performed to determine the sequence of the CEF levels, and two models were proposed: $\Gamma_8(0) - \Gamma_6(4.7) - \Gamma_7(11\text{ K})$ and $\Gamma_8(0) - \Gamma_7(3.5) - \Gamma_6(10.3\text{ K})$.[22] One of the purposes of the above analysis is to decide which of the two is correct. Figure 4 shows the calculated strain susceptibilities for the two sequences. Although the two sequences give different strain susceptibilities, it is possible to fit the data for both sequences by choosing the proper parameters of g_Γ and $g_\Gamma{}'$ that are not so much different from the above values. It is also possible to fit the data even if Γ_8 is located at the first excited state. This model gives the Van Vleck type strain susceptibility at low temperatures. C_{44} deviates from the Curie type behavior below 6 K and it is possible to ascribe this deviation to the Van Vleck type behavior due to the Γ_8 excited state. However, this model can not explain other experimental results and was also discarded from the neutron scattering result. What we can say from the above fitting is that the total CEF splitting is very small if existed as has been estimated from other measurements, and that

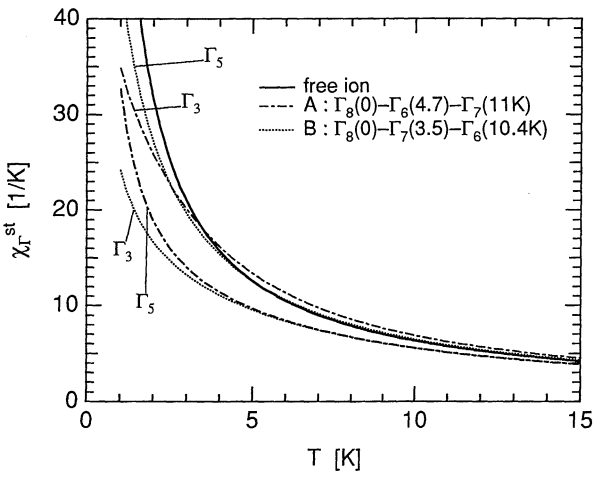

Fig. 4. Temperature dependences of the quadrupolar strain susceptibility for two CEF models and for a free Tm^{2+} ion. A free ion has no distinction between Γ_3 and Γ_5.

the sign of the inter-ionic quadrupolar interaction $g_\Gamma{}'$ is minus, indicating the antiferro inter-ionic quadrupolar interactions.

It would be worthwhile to compare the above obtained coupling constants with those of CeTe, which is the only rare earth monotelluride for which g_Γ and $g_\Gamma{}'$ have been determined so far.[32] The normalized values are listed in Table II, where α_J is the Stevens factor and $\langle r^2\rangle$ is the second moment of the radial $4f$ wavefunction.[33,34] The single ion quadrupole-strain coupling constants of TmTe are larger than those of CeTe. It should be noted that CeTe is a trivalent metal with one conduction electron per one Ce ion while TmTe is a divalent insulator. At any rate, the knowledge on the quadrupole-strain interactions of other monochalcogenides is lacking.

The bulk modulus C_B shows a normal temperature dependence with no particular anomaly. This is because ε^α with Γ_1 symmetry does not break the symmetry of the system and therefore induces no splitting in the CEF levels. C_{44} deviates from the theoretical line below about 6 K, while $(C_{11} - C_{12})/2$ follows the theoretical line down to about 2.5 K, a temperature just above the phase transition. Furthermore, the cusp at 1.8 K is sharp for $(C_{11} - C_{12})/2$ while it is relatively broad for C_{44}. These differences are possibly related with the order parameter and its fluctuations as the temperature approaches the critical point.

3.2 specific heat

In this section we investigate the phase transition of 1.8 K from the specific heat. Figure 5 shows the spe-

Table II. Comparison of the coupling constants between TmTe and CeTe.

		CeTe	TmTe
$\lvert g_{\Gamma_3}\rvert/\alpha_J\langle r^2\rangle$	[K/Å^2]	6.7×10^3	9.0×10^3
$g_{\Gamma_3}'/(\alpha_J\langle r^2\rangle)^2$	[K/Å^4]	2.7×10^2	-5.1×10^3
$\lvert g_{\Gamma_5}\rvert/\alpha_J\langle r^2\rangle$	[K/Å^2]	5.7×10^3	1.2×10^4
$g_{\Gamma_5}'/(\alpha_J\langle r^2\rangle)^2$	[K/Å^4]	-8.4×10^3	-1.5×10^3

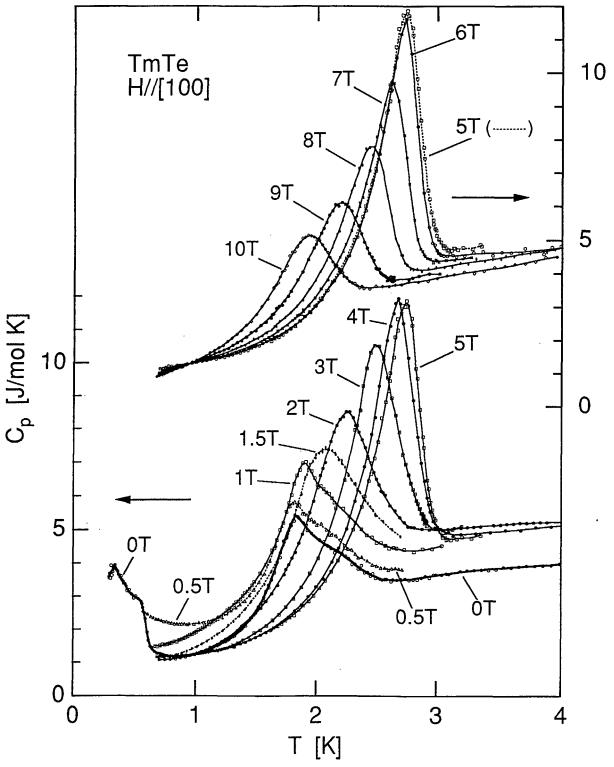

Fig. 5. Specific heat of TmTe under magnetic fields along the [100] axis.

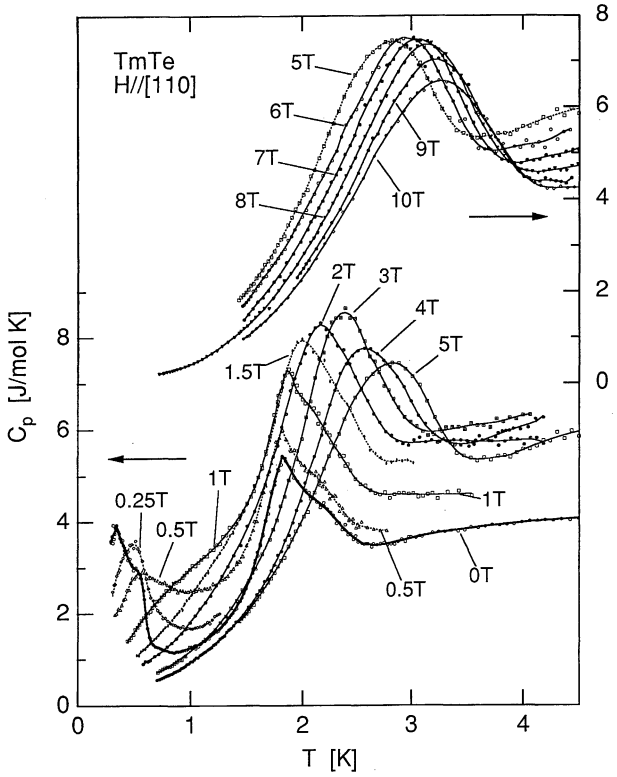

Fig. 6. Specific heat of TmTe under magnetic fields along the [110] axis.

cific heat of TmTe under magnetic fields along the [100] axis. The anomaly at 1.8 K and 0 T corresponds to the phase transition which is also observed as the cusps in the elastic constants. Another anomaly around 0.5 K corresponds to the AFM ordering. The specific heat peak at 1.8 K and 0 T is small and has a relatively long tail to the high temperature side. By applying the magnetic field, the transition temperature shifts to higher temperatures and the specific heat peak becomes sharper and larger. The long tail at 0 T gradually disappears with increasing the field. Above 5 T, on the contrary, the transition temperature decreases with increasing field and the peak becomes weaker and broader. It should be taken into consideration that the peak looks round when crossing the slanted phase line. For example, the peak for 0 T is broad and has a long tail but the top of which is sharp. On the other hand, the top of the 1.5 T's peak is round.

Figures 6 and 7 show the specific heat under magnetic fields along the [110] and [111] axes, respectively. At low fields the specific heat peaks become larger with increasing the field and the transition temperature shifts to higher temperatures. However, at high fields above 4 T, the overall behavior is very different from that for $H \parallel [100]$. The most remarkable difference is that the peaks, especially for $H \parallel [111]$, are much broader than those for $H \parallel [100]$. The $(H - T)$ phase diagram of TmTe was deduced from these peak temperatures, and is shown in Fig. 8. This phase diagram is very similar to that of CeB_6 in which the occurrence of the antiferro quadrupolar ordering has already been established.[35,36] In CeB_6, however, the closing of the phase line has not yet been observed.

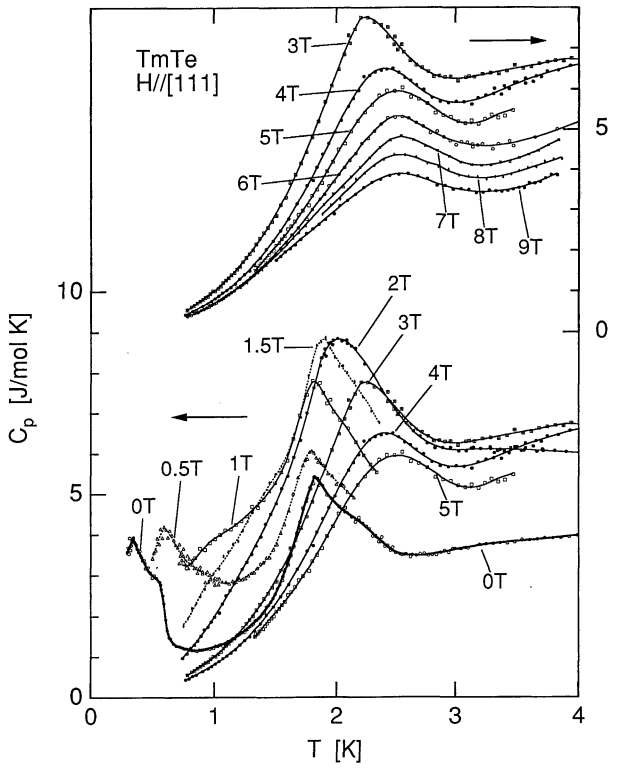

Fig. 7. Specific heat of TmTe under magnetic fields along the [111] axis.

The AFM transition below 0.5 T seems to have two steps: a sharp turn at 0.34 K and a shoulder around 0.5 K. This two step transition can also be seen in the magnetic susceptibility in Fig. 1, though the correspond-

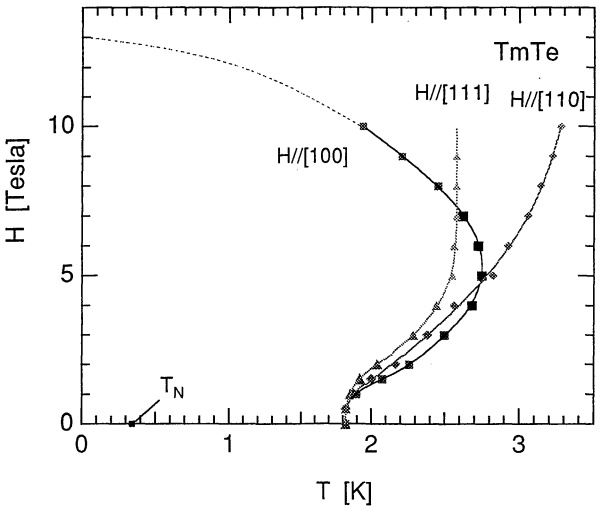

Fig. 8. $(H - T)$ phase diagram deduced from the specific heat peaks. The size and the darkness of the marks represent the sharpness of the specific heat peaks. Dotted lines above 10 T are the speculations. With regard to T_N, the temperature where the specific heat showed a sharp cusp is plotted only for $H = 0$ T.

ing temperatures are different. The AFM ordering seems to disappear by a small field of several kilogauss. From Figs. 6 and 7, it seems that the sharp peak at 0.34 K and 0 T disappears by applying a weak magnetic field while the shoulder at 0.5 K remains. At any rate, the details on the magnetic ordering under magnetic fields are unknown because of the lack of the measurement down to the lower temperatures. However, it should be noted that the specific heat for $H \parallel [110]$ and $H \parallel [111]$, under magnetic fields higher than 3 or 4 T, decreases down to zero with decreasing temperature. On the other hand, for $H \parallel [100]$, the specific heat does not decrease to zero even at 10 T, indicating that some entropy still remain below 0.5 K.

Figure 9 shows the magnetic part of the specific heat of TmTe at high temperatures in the paramagnetic region. The specific heat of YbTe was subtracted as the contribution from the lattice. At zero field, a broad peak is observed around 5 K that is considered to be a Schottky specific heat of the CEF levels. However, this peak can not be explained in terms of the single site CEF model with the total splitting less than 15 K. A calculated Schottky specific heat for one of the proposed CEF models is shown in the figure as an example. The most remarkable discrepancy is that the calculated Schottky specific heat decreases rapidly above 5 K with increasing the temperature while the real system has a long tail that is still very large even at high temperatures from 20 K to 30 K. This means that the f electrons begin to lose their degree of freedom below a temperature much higher than the single site CEF splitting or the ordering temperature of 1.8 K.

Figure 10 shows the variations of the entropy as a function of temperature for $H \parallel [111]$. We were not able to estimate the entropy for $H \parallel [100]$ because the specific heat did not decrease to zero even under high magnetic fields. The entropy apparently exceed $R \ln 6$ and approaches $R \ln 8$, which is the total entropy of a Tm^{2+}

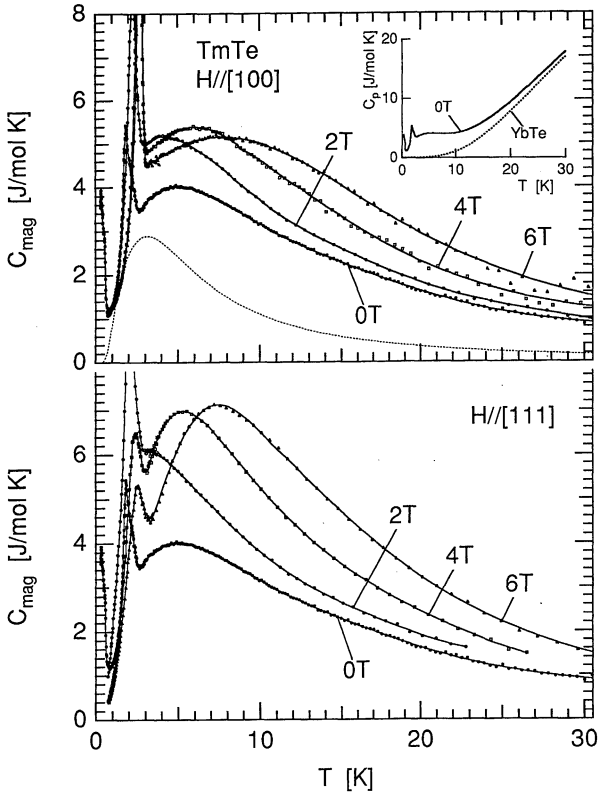

Fig. 9. Specific heat of TmTe after the subtraction of YbTe as the lattice contribution. The dotted line in the upper figure represents the calculated Schottky specific heat for the CEF model of $\Gamma_8(0) - \Gamma_6(4.7) - \Gamma_7(11\ \mathrm{K})$.

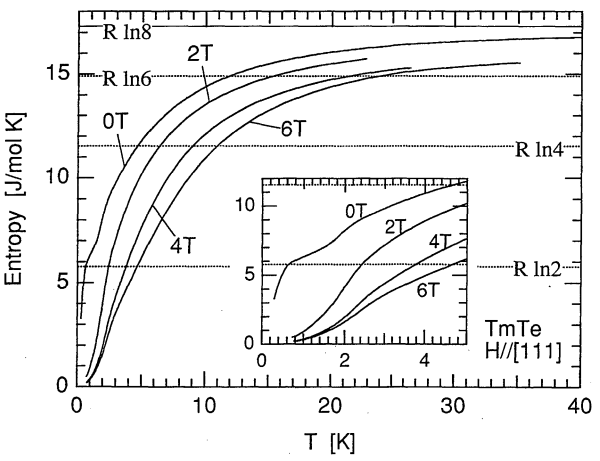

Fig. 10. Variation of the magnetic entropy of TmTe as a function of temperature for $H \parallel [111]$, which is the field direction the specific heat decreased to zero under magnetic fields. The absolute value for 0 T was estimated by extrapolating the specific heat linearly to zero toward absolute zero temperature.

ion with $J = 7/2$. The inset shows the low temperature part of the entropy variation. At the phase transition temperature of 1.8 K, the entropy for 0 T apparently exceeds $R \ln 2$ though it is less than $R \ln 4$. If we take into account that the the specific heat peak for 0 T has a tail up to about 4 K and that the entropy reaches $R \ln 4$ around 5 K, the ground state is supposed to be a quartet. This result also supports the Γ_8 ground state model.

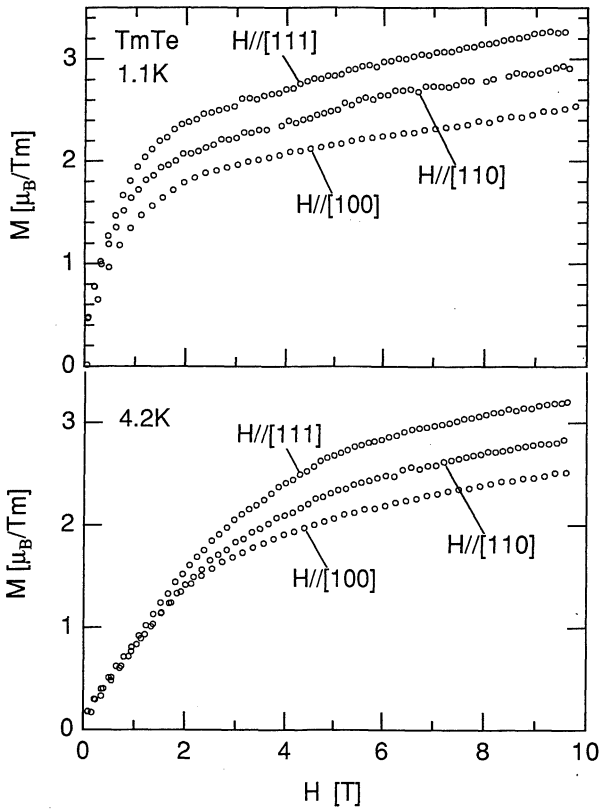

Fig. 11. Magnetization of TmTe for the tree main crystal axes.

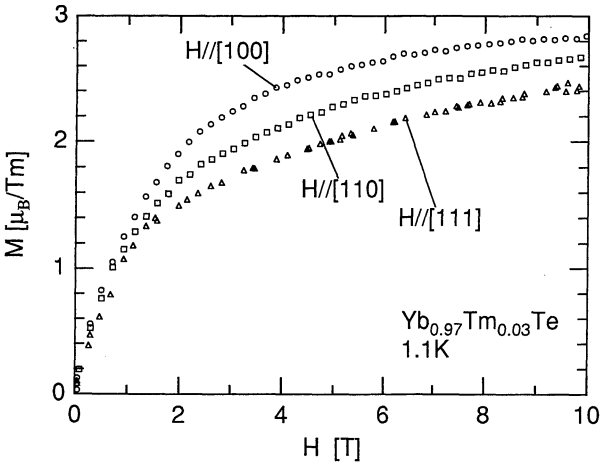

Fig. 12. Magnetization of $Yb_{0.97}Tm_{0.03}Te$ at 1.1 K in the paramagnetic region.

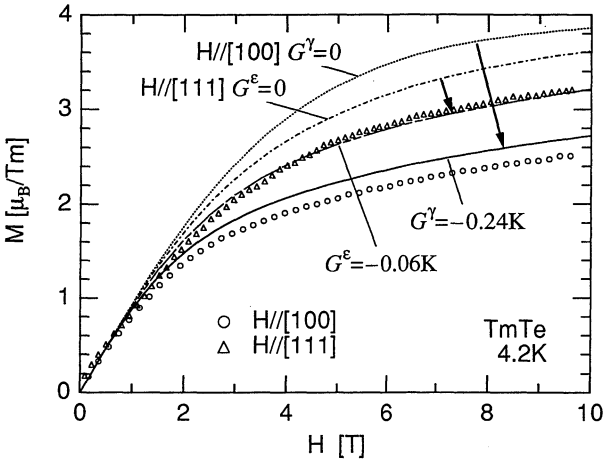

Fig. 13. Calculated magnetization curves considering CEF, quadrupole-strain, inter-ionic quadrupolar interactions, and elastic energy. $\Gamma_8(0)-\Gamma_6(4.7)-\Gamma_7(11\ \mathrm{K})$ was assumed as single site CEF levels. The curves for $G_\Gamma = 0$ are the calculations without the considerations of the quadrupolar effects.

3.3 magnetization

The magnetization curves of TmTe for the three main directions at 1.1 K and 4.2 K are shown in Fig. 11. The magnetization along the [111] axis is the largest and along the [100] axis the smallest for the both temperatures. The magnetization curves at 4.2 K behave like those of a Brillouin function, while those at 1.1 K, an intermediate temperature between the two transition temperatures, show relatively linear increase above 1 T. The reason for this behavior may be that the direction of the magnetic moments is restricted by the ordering of the quadrupolar moments below 1.8 K.

On the other hand, in a diluted system of $Yb_{0.97}Tm_{0.03}Te$, the sequence of the easy axis of magnetization is reversed as shown in Fig. 12; [100] becomes the easy axis and [111] becomes the hard axis. This change in the sequence of the easy axis is also the case for $La_{1-x}Ce_xB_6$.[37]

The magnetization is suppressed below 3 μ_B in the experiment, while the saturation moment of a Tm^{2+} ion is 4 μ_B. One of the possible explanations is to consider the effect of the quadrupolar moments. Jausaud *et al.* explained the magnetization of TmCu by considering the quadrupole-strain interaction, inter-ionic quadrupolar interaction and the elastic energy in the mean field approximation.[38] In this formalism these interactions associated with the quadrupolar moments are summarized in one parameter G_Γ, which is written as $G_\Gamma = Ng_\Gamma^2/C_\Gamma + g_\Gamma'$. For the magnetic field along the [100] axis, the Hamiltonian can be written as

$$\mathcal{H}^\gamma = N[\mathcal{H}_{\mathrm{CEF}} + g\mu_B J_z(H+\lambda M) - G^\gamma O_2^0\langle O_2^0\rangle] + \frac{1}{2}\lambda M^2 + \frac{1}{2}C_{\Gamma_1}^0(\varepsilon^\alpha)^2 + \frac{N}{2}G^\gamma\langle O_2^0\rangle^2, \quad (3.4)$$

and for the field along the [111] axis,

$$\mathcal{H}^\varepsilon = N[\mathcal{H}_{\mathrm{CEF}} + \frac{1}{\sqrt{3}}g\mu_B(J_x+J_y+J_z)(H+\lambda M) - G^\varepsilon(O_{yz}+O_{zx}+O_{xy})\langle O_{xy}\rangle] + \frac{1}{2}\lambda M^2 + \frac{1}{2}C_{\Gamma_1}^0(\varepsilon^\alpha)^2 + \frac{3N}{2}G^\varepsilon\langle O_{xy}\rangle^2. \quad (3.5)$$

The quadrupolar moment $\langle O_2^0\rangle$ is induced for $H \parallel [100]$, and $\langle O_{xy}\rangle (= \langle O_{yz}\rangle = \langle O_{zx}\rangle)$ is induced for $H \parallel [111]$. N is the number of ions in a unit volume and $\lambda = \theta_p/(\text{Curie constant})$ is the mean field coefficient for the magnetization. The calculated magnetization curves in this formalism are shown in Fig. 13. λ was assumed to be zero because θ_p is small in this material. The curves for $G_\Gamma = 0$ show only the CEF effect. Taking into account the G_Γ parameter, which was calculated from the pa-

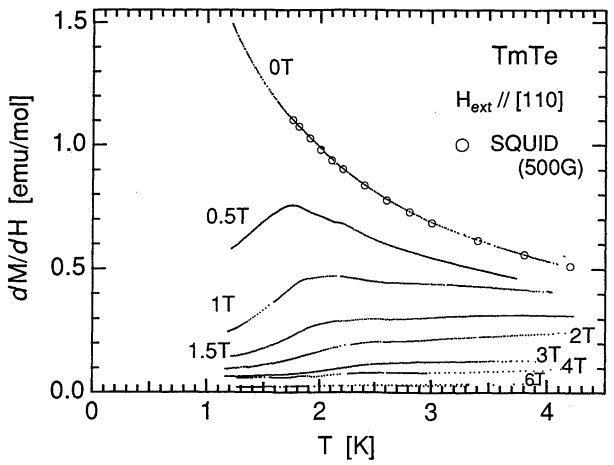

Fig. 14. Temperature dependence of dM/dH under static magnetic fields. Absolute values were determined by fitting the results for 0 T to the DC susceptibility measeured with a SQUID magnetometer at 500 G.

rameters obtained in the fitting of the elastic constants, we can explain not only the suppressions but also the change in the easy axis. However, this model can not explain the magnetization curves of $Yb_{0.97}Tm_{0.03}Te$, which is also suppressed below 3 μ_B even at 10 T. These suppressions can be explained in this formalism only by the G_Γ parameters with minus sign, which may not be the case for $Yb_{0.97}Tm_{0.03}Te$ because of the weak inter-ionic quadrupolar interactions that lead to small values of $g_\Gamma{}'$. Furthermore, this model can not explain the specific heat of TmTe; the calculated absolute values are smaller than the experimental results, especially at high temperatures where the large tail appears in the experiment.[27]

We have also measured the magnetization of TmTe at 2.15 K to detect an anomaly when crossing the phase line. However, we could not observe any clear anomaly in the magnetization curve at 2.15 K in spite that the sample clearly crossed the phase line vertically. It was also the case for the elastic constants. In the magnetic field scans of C_{44} and $(C_{11}-C_{12})/2$ at a temperature of 2.4 K and 2.2 K, respectively, no sharp anomalies were observed but a hysteresys with a broad width about 3 T. On the other hand, in the temperature scans of the elastic constants under magnetic fields, the cusps were observed at the transition temperatures that are consistent with Fig. 8.

In §3.1 we described that the magnetic susceptibility showed no anomaly at the phase transition of 1.8 K. By applying a weak magnetic field, however, the magnetic susceptibility shows a cusp. Figure 14 shows the temperature dependence of dM/dH of TmTe measured with an AC technique under static magnetic fields along the [110] axis. Absolute values were determined by fitting the result for 0 T to the DC susceptibility measured with a SQUID magnetometer. At 0 T dM/dH showed no anomaly at 1.8 K as we have seen in Fig. 1. At 0.5 T, however, dM/dH showed a cusp at 1.8 K. Though the cusp become invisible at high fields, it shifts to higher temperatures consistently with the $(H-T)$ phase diagram. This experimental result is related with the third order magnetic susceptibility. If we write the magnetization process as $M=\chi_1 H+\chi_3 H^3+\cdots$, dM/dH can be written as $\chi_1+3\chi_3 H^2+\cdots$. The cusp in dM/dH at 0.5 T indicates an anomaly in χ_3. However, more detailed measurement is needed to discuss χ_3.

§4. Discussions

The phase transition at 1.8 K may be classified as an antiferro quadrupolar (AFQ) ordering from the following reasons. Firstly, as we described in §3.1, only the degeneracy of the quadrupolar moment is lifted below the phase transition at 1.8 K while the magnetic degeneracy, the Kramers doublet, remains. Secondly, the sign of $g_\Gamma{}'$, the coupling constant of the inter-ionic quadrupolar interaction in the mean field approximation, is minus. Thirdly, the way in which the ordering is enhanced by the magnetic field is very similar to that of the AFQ ordering in CeB_6, which has already been established. In the case of CeB_6, magnetic Bragg peaks associated with a wave vector $\boldsymbol{q}=(1/2,1/2,1/2)$ are induced by applying magnetic fields, though it is invisible at zero field. This anomalous result has been explained by the existence of the ordered quadrupolar moments with this $\boldsymbol{q}$ vector and has been considered as the evidence of the AFQ ordering in CeB_6.[35] Recently, neutron scattering experiment under magnetic fields has also been performed on TmTe. It was found that new magnetic Bragg peaks associated with a wave vector $\boldsymbol{q}=(1/2,1/2,1/2)$ were induced under magnetic fields.[39] This can be a conclusive evidence of the AFQ ordering in TmTe.

The AFM ordering occurs in the AFQ phase at $T_N(<T_Q=1.8$ K). Therefore, the magnetic structure of the AFM phase must be consistent with the AFQ ordering. From this standpoint, the wave vector $\boldsymbol{q}=(1/2,1/2,1/2)$ for the AFM structure in TmTe seems too simple; this $\boldsymbol{q}$ vector is the same as that of the AFQ phase. In the case of CeB_6, the AFM phase has a double $\boldsymbol{q}$ structure with $\boldsymbol{q}_1=(1/4,1/4,1/2)$ and $\boldsymbol{q}_2=(1/4,-1/4,1/2)$, which is consistent with the order parameter of the AFQ phase. Because the quadrupolar ordering restricts the possible direction of the accompanying magnetic moments, the $\boldsymbol{q}$ vector of the magnetic ordering should have the component such as 1/4 if the $\boldsymbol{q}$ vector of the AFQ phase was $(1/2,1/2,1/2)$.

We have pointed out that we can not explain the high temperature part of the specific heat and the magnetization curves simultaneously in the mean field approximation. The entropy decreases with decreasing temperature much faster than that expected from the single site CEF model. This suggests the existence of a short range ordering or fluctuations in this temperature range much higher than T_Q. With regard to this point, Triplett *et al.* reported an important result of the Mössbauer absorption on TmTe.[40] They observed non-zero nuclear quadrupole splittings in the absorption spectra below 40 K, which is much higher than T_Q. They concluded from their experimental result that the Tm site symmetry can not be cubic even in the paramagnetic temperature region. We consider this symmetry lowering to be caused by the onset of the short range quadrupolar ordering or by the fluctuations of the local symmetry

among the stable distortions (dynamic Jahn-Teller effect). These effect must be taken into account in the analysis not only of the specific heat but also of other physical properties at high temperatures. The Schottky-like specific heat peak around 5 K, therefore, is considered to be caused not only by the single site CEF but also by some kind of fluctuation that appear in the process of the local distortion developing into the coherent long range AFQ ordering at 1.8 K. The deviation of C_{44} from the theoretical line below 6 K, as well as the considerably larger quasielastic and inelastic line widths than the instrumental resolution in neutron scattering, as pointed out in ref. 22, is supposed to be related with the above effect that may accompany unstabilized Γ_8.

One of the most important characteristics of the AFQ ordering in TmTe is its anomalous $(H-T)$ phase diagram which is shown in Fig. 8. Magnetic fields are normally against orderings when the symmetry of the ordered phase is different from that of the magnetic field. Therefore, for example, the transition temperature of an antiferro magnet normally decreases with increasing the magnetic field. There have been some theoretical approaches so far concerning the problem of the anomalous $(H-T)$ phase diagrams in CeB_6 and TmTe.[41-45] Experimentally, various interesting phase diagrams have recently been reported on the $La_{1-x}Ce_xB_6$ system.[46-50] Though we have pointed out in this paper some features that are similar between CeB_6 and TmTe, there also are different features that should be noted. The first point is the anisotropy of T_Q. If we compare the phase diagram of CeB_6 with that of TmTe below 5 T, $T_Q^{[111]} < T_Q^{[110]} < T_Q^{[100]}$ for TmTe while $T_Q^{[100]} < T_Q^{[111]} < T_Q^{[110]}$ for CeB_6.[50] In addition, the specific heat peaks of CeB_6 at T_Q are very sharp for every field directions, while those of TmTe is sharp only for $H \parallel [100]$. The second point is that the softening of C_{44} in CeB_6 well follows the theoretical curve down to $T_Q = 3.3$ K,[31] while that of TmTe deviates from the theoretical curve below about 6 K. This unusual behavior in C_{44} suggests O_{xy} to be the order parameter that accompany large fluctuations. However, it is a subject that should be clarified in future. Thirdly, the $\boldsymbol{q}$ vector of the AFM phase is different. As we pointed out above, the consistency of the order parameter between the AFM phase and the AFQ phase in TmTe is an open problem.

Finally, we would like to comment about the magnetic ordering. Several authors have reported different T_N for TmTe from different kinds of measurement with different samples. Bucher *et al.*, as well as Ott and Fulliger, reported $T_N \sim 0.23$ K from the AC susceptibility result. This value is in accord with our result of the AC susceptibility. Lassailly *et al.* reported $T_N = 0.43$ K from neutron scattering. This difference has so far been ascribed to the different quality of the samples. However, in this paper, we have measured the specific heat and the AC susceptibility of TmTe using the same sample and have obtained the results that are shown in Figs. 1 and 5. Though we have found two step anomaly of the AFM ordering in TmTe both in the AC susceptibility and the specific heat, the corresponding temperatures did not agree with each other. The cause of this disagreement is not clear yet and more detailed study is necessary.

§5. Conclusion

We have prepared a high quality single crystal of TmTe and have measured the various physical properties at low temperatures. We have found for the first time the occurrence of the antiferro quadrupolar ordering in TmTe. The transition temperature of $T_Q = 1.8$ K is almost four times higher than the Néel temperature, indicating the importance of the quadrupolar interactions in TmTe. Furthermore, it is difficult to explain the specific heat result in the temperature region above T_Q within the mean field theory.

This AFQ transition has many similar characters to that of CeB_6, as well as many different characters. The magnetic susceptibility shows no clear anomaly at $T_Q = 1.8$ K, while the elastic constants show the cusps. The detailed measurement of the specific heat under magnetic fields revealed the unusual $(H-T)$ phase diagram. In particular, for $H \parallel [100]$, the closing of the phase line was observed, which has not yet been observed in CeB_6. The specific heat peaks under magnetic fields are very sharp for $H \parallel [100]$, while they are broad for $H \parallel [110]$ and $H \parallel [111]$. The magnetization of TmTe along the [111] axis gives the largest values and along the [100] axis gives the smallest, while the sequence is reversed in the diluted system of $Yb_{0.97}Tm_{0.03}Te$, as is the case for CeB_6.

Though O_{xy} is expected to be the order parameter of the AFQ phase in TmTe, it must be determined experimentally in future. Many kinds of experiments are necessary to reveal the mechanism of the antiferro quadrupolar ordering of this material.

Acknowledgements

The authors would like to express sincere thanks to Mr. Y. Nemoto and Dr. K. Morita for their help with the experiments, Dr. E. Clementyev, Dr. I. Goncharenko, Dr. P. Link, Dr. M. Braden and Dr. J. M. Mignot for valuable discussions and Dr. P. Haen for important information of unpublished results. This work has been supported by Grant-in-Aids No. 07404016 from the Ministry of Education, Science and Culture of Japan. T. M. has been supported by JSPS research fellowships for young scientists.

1) E. Bucher, K. Andres, F. J. di Salvo, J. P. Maita, A. C. Gossard, A. S. Cooper and G. W. Hull, Jr.: Phys. Rev. B **11** (1975) 500.
2) N. Kioussis, B. R. Cooper and J. M. Wills: Phys. Rev. B **44** (1991) 10003.
3) E. Kaldis and P. Wachter: Solid State Commun. **11** (1972) 907.
4) B. Batlogg, E. Kaldis, A. Schlegel and P. Wachter: Phys. Rev. B **14** (1976) 5503.
5) R. Suryanarayanan, G. Güntherodt, J. L. Freeouf and F. Holtzberg: Phys. Rev. B **12** (1975) 4215.
6) K. Andres, W. M. Walsh, Jr., S. Darack, L. W. Rupp, Jr. and L. D. Longinotti: Solid State Commun. **27** (1978) 825.
7) B. Batlogg, H. R. Ott, E. Kaldis, W. Thöni and P. Wachter: Phys. Rev. B **19** (1979) 247.
8) P. Haen, F. Lapierre, J. M. Mignot, R. Tournier and F.

Holtzberg: Phys. Rev. Lett. **43** (1979) 304.
9) G. Chouteau, F. Holtzberg, O. Peña, T. Penney and R. Tournier: J. Phys. (Paris) **40** (1979) C5-361.
10) H. B. Moller, S. M. Shapiro and R. J. Birgeneau: Phys. Rev. Lett. **39** (1977) 1021.
11) P. Haen, F. Holtzberg, F. Lapierre, T. Penney and R. Tournier: *Valence Instabilities and Related Narrow Band Phenomena,* ed. R. D. Parks (Plenum, New York, 1977) p. 495.
12) M. Loewenhaupt and E. Holland-Moritz: J. Appl. Phys. **50** (1979) 7456.
13) E. Holland-Moritz: J. Magn. Magn. Mater. **38** (1983) 253.
14) S. M. Shapiro and B. H. Grier: Phys. Rev. B **25** (1982) 1457.
15) A. Berger, E. Bucher, P. Haen, F. Holtzberg, F. Lapierre, T. Penney and R. Tournier: *Valence Instabilities and Related Narrow Band Phenomena,* ed. R. D. Parks (Plenum, New York, 1977) p. 491.
16) P. Haen, H. Bioud, F. Lapierre and F. Holtzberg: *Theoretical and Experimental Aspects of Valence Fluctuations, Proc. 5th. Int. Conf. on Valence Fluctuations, Bangalore, 1987* ed. L. C. Gupta and S. K. Malik (Plenum, New York, 1987) p. 445.
17) F. Holtzberg, J. Flouquet, P. Haen, F. Lapierre, Y. Lassailly and C. Vettier: J. Appl. Phys. **57** (1985) 3152.
18) J. Neuenschwander and P. Wachter: Phys. Rev. B **41** (1990) 12693.
19) T. Matsumura, T. Kosaka, J. Tang, T. Matsumoto, H. Takahashi, N. Môri and T. Suzuki: Phys. Rev. Lett. **78** (1997) 1138.
20) H. R. Ott, B. Lüthi and P. S. Wang: *Valence Instabilities and Related Narrow Band Phenomena,* ed. R. D. Parks (Plenum, New York, 1977) p. 289.
21) H. R. Ott and B. Lüthi: Z. Phys. B **28** (1977) 141.
22) E. Clementyev, R. Köhler, M. Braden, J.-M. Mignot, C. Vettier, T. Matsumura and T. Suzuki: Physica B **230–232** (1997) 735.
23) H. R. Ott and F. Hulliger: Z. Phys. B **49** (1983) 323.
24) Y. Lassailly, C. Vettier, F. Holtzberg, A. Benoit and J. Flouquet: Solid State Commun. **52** (1984) 717.
25) T. Matsumura, Y. Haga, Y. Nemoto, S. Nakamura, T. Goto and T. Suzuki: Physica B **206&207** (1995) 380.
26) T. Matsumura, S. Nakamura, T. Goto, H. Shida and T. Suzuki: Physica B **223&224** (1996) 385.
27) T. Matsumura, H. Shida and T. Suzuki: Physica B **230&232** (1997) 738.
28) M. Kataoka and J. Kanamori: J. Phys. Soc. Jpn. **32** (1972) 113.
29) V. Dohm and P. Fulde: Z. Phys. B **21** (1975) 369.
30) P. M. Levy: J. Phys. C **6** (1973) 3545.
31) S. Nakamura, T. Goto, S. Kunii, K. Iwashita and A. Tamaki: J. Phys. Soc. Jpn. **63** (1994) 623.
32) H. Matsui, T. Goto, A. Tamaki, T. Fujimura, T. Suzuki and T. Kasuya: J. Magn. Magn. Mater. **76&77** (1988) 321.
33) K. W. H. Stevens: Proc. Phys. Soc. London A **65** (1952) 209.
34) A. J. Freeman and J. P. Desclaux: J. Magn. Magn. Mater. **12** (1979) 11.
35) J. M. Effantin, J. Rossat-Mignod, P. Burlet, H. Bartholin, S. Kunii and T. Kasuya: J. Magn. Magn. Mater. **47&48** (1985) 145.
36) W. A. C. Erkelens, L. P. Regnault, P. Burlet, J. Rossat-Mignod, S. Kunii and T. Kasuya: J. Magn. Magn. Mater. **63&64** (1987) 61.
37) N. Sato, S. Kunii, I. Oguro, T. Komatsubara and T. Kasuya: J. Phys. Soc. Jpn. **53** (1984) 3967.
38) C. Jaussaud, P. Morin and D. Schmitt: J. Magn. Magn. Mater. **22** (1980) 98.
39) P. Link *et al.*: to be published.
40) B. B. Triplett, Y. Mahmud, N. S. Dixon, S. S. Hanna and F. Holtzberg: Phys. Lett. A **67** (1978) 151.
41) F. Ohkawa: J. Phys. Soc. Jpn. **52** (1983) 3897.
42) F. Ohkawa: J. Phys. Soc. Jpn. **54** (1985) 3909.
43) R. Shiina, H. Shiba and P. Thalmeier: J. Phys. Soc. Jpn. **66** (1997) 1741.
44) G. Uimin, Y. Kuramoto and N. Fukushima: Solid State Commun. **97** (1996) 595.
45) K. Hanzawa and T. Kasuya: J. Phys. Soc. Jpn **53** (1984) 1809.
46) M. Hiroi, S. Kobayashi, M. Sera, N. Kobayashi and S. Kunii: J. Phys. Soc. Jpn **66** (1997) 1762.
47) T. Sakakibara, T. Tayama, H. Amitsuka, K. Tenya, S. Kunii, T. Suzuki and A. Ochiai: Physica B **230–232** (1997) 307.
48) S. Nakamura, T. Goto and S. Kunii: J. Phys. Soc. Jpn. **64** (1995) 3941.
49) S. Nakamura, O. Suzuki, T. Goto, S. Sakatsume, T. Matsumura and S. Kunii: J. Phys. Soc. Jpn. **66** (1997) 552.
50) M. Hiroi, M. Sera, N. Kobayashi and S. Kunii: Phys. Rev. B **55** (1997) 8339.